Flux-quantum-discretized dynamics of magnetic flux entry, exit, and annihilation in current-driven mesoscopic type-I superconductors

G. R. Berdiyorov,[1] A. D. Hernández-Nieves,[1,2] M. V. Milošević,[1] F. M. Peeters,[1,*] and D. Domínguez[2]
[1]*Departement Fysica, Universiteit Antwerpen, Groenenborgerlaan 171, B-2020 Antwerpen, Belgium*
[2]*Centro Atomico Bariloche, 8400 San Carlos de Bariloche, Rio Negro, Argentina*
(Received 6 January 2012; published 7 March 2012)

We study nonlinear flux dynamics in a current-carrying type-I superconductor. The stray magnetic field of the current induces the intermediate state, where nucleation of flux domains is *discretized to a single fluxoid at a time*, while their final shape (tubular or laminar), size, and nucleation rate depend on applied current and edge conditions. The current induces opposite flux domains on opposite sides of the sample, and subsequently drives them to annihilation—which is *also discretized*, as a sequence of vortex-antivortex pairs. The discretization of both nucleation and annihilation leaves measurable traces in the voltage across the sample and in locally probed magnetization. The reported dynamic phenomena thus provide an unambiguous proof of a flux quantum being the smallest building block of the intermediate state in type-I superconductors.

DOI: 10.1103/PhysRevB.85.092502 PACS number(s): 74.78.Na, 73.23.−b, 74.25.fc, 74.25.Uv

The intermediate state (IS) of type-I superconductors recently attracted renewed interest,[1–6] being a very rich study object. It consists of coexisting flux-bearing normal and flux-prohibitive superconducting domains, formed in patterns which balance the short-range attractive force due to interfacial tension and the long-range repulsive magnetic interaction between the domains. While in some cases the structure of the IS resembles the Landau picture,[7] i.e., a periodic structure of alternating stripes of normal and superconducting phases,[8] very often much more complex patterns are observed, especially in the case of different magnetic history or sample geometry.[1,2] Sample size is also of importance, as IS becomes even richer in the mesoscopic regime where confinement can cause different flux patterns.[4–6]

Arguably the most popular theoretical model for the bulk IS is the "current loop" model,[9] which nicely describes the pattern formation if the internal structure of flux domains is entirely neglected. However, one must raise the question of the possible internal structure considering that domains, regardless of their shape, must be flux quantized. At the same time, despite the increased number of experimental and theoretical works, a complete description of the nucleation of the IS domains, as quantized objects, is still lacking. The same holds for domain interactions with, e.g., hole, boundary, or another domain, where, bear in mind, quantization should remain preserved. References 10–12 employed the time-dependent Ginzburg-Landau (TDGL) theory to study the nucleation of the superconducting phase in type-I long cylinders in a parallel magnetic field, and reported interesting transient patterns during a field quench from the normal state. However, these structures are different from those arising due to demagnetization (which does not exist for infinite cylindrical samples). To our knowledge, only the work by Bokil and Narayan[13] addressed flux penetration into type-I superconductors with demagnetization effects taken into account. Their main finding was the instability in the process, resulting in flux penetration as a series of bursts, and the formation of isolated normal droplets. However, authors used the sharp interface model, which similarly to the loop model neglects the spatial variation of the order parameter. Furthermore, the calculation was done with lattice spacing larger than the coherence length, so that the fine features of the domains and their formation were impossible to observe.

Another degree of complexity is added to the problem in the presence of an applied electric current. It is known, for example, that laminar patterns split into highly mobile tubular structures[14] and evolve into equally spaced superconducting walls in increasing current.[7,14] A recent experiment[3] on a narrow channel in a type-I superconducting stripe suggested that a chain of flux domains can undergo different dynamic phases, where the linear motion of domains can be periodic (with single or multiple periods) as well as chaotic. To our knowledge, no theoretical reports addressed the IS dynamics in type-I samples, neither its nucleation and growth discussed above, nor its current-induced topological transformations and kinematic phases. Therefore, in this work, we do exactly that—we examine the behavior of the IS flux structures in a type-I slab subjected to an applied current (in the absence of other magnetic fields). As we will show, the dynamics of both nucleation and interaction of flux domains reveals their *discrete nature*, both occurring via individual flux quanta. We explain how our findings are directly verifiable in transport and magnetic measurements, and how they relate to other experiments, e.g., the one of Ref. 3.

Figure 1 depicts the geometry of our sample—a type-I superconducting slab with dimensions $L \times w \times d$, with an external current I applied in the x direction. For this system, we solved the generalized TDGL equations,[15,16]

$$\frac{u}{\sqrt{1+\gamma^2|\psi|^2}}\left(\frac{\partial}{\partial t}+\frac{\gamma^2}{2}\frac{\partial|\psi|^2}{\partial t}\right)\psi = (\nabla - i\mathbf{A})^2\psi + \psi - \psi^3, \quad (1)$$

$$\kappa^2 \mathrm{rot}\ \mathrm{rot}\mathbf{A} = \mathrm{Re}[\psi^*(-i\nabla - \mathbf{A})\psi] - \frac{\partial \mathbf{A}}{\partial t} \equiv \mathbf{J}. \quad (2)$$

These equations are derived from the microscopic theory in the local approximation, $\xi(T),\lambda(T) > l_e$, where $\xi(T)$ and $\lambda(T)$ are the temperature-dependent coherence length and penetration depth, respectively, and l_e is the scattering length. This condition of locality is obviously easily satisfied close

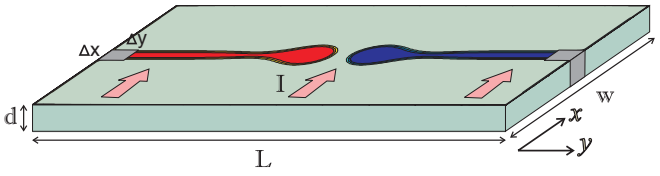

FIG. 1. (Color online) The studied system: A superconducting slab (width w, length L, and thickness d) with two edge defects (size $\Delta x \times \Delta y$) and an external current I.

to the critical temperature T_c, which is also the domain of applicability of the TDGL theory (see Table I of Ref. 16 for the validity range in the case of several type-I superconductors). In our approach, we neglected the thermal fluctuations because the Ginzburg number, governing the strength of the thermal fluctuations, is directly proportional to T_c and κ^2,[17] and therefore must be very small in the type-I samples of interest in our study. In Eqs. (1) and (2), distance is scaled to $\xi(T)$, the vector potential $\mathbf{A}$ is in units of $\Phi_0/2\pi\xi(T)$, time is in units of the GL relaxation time $t_{\rm GL} = \pi\hbar/8k_B(T_c - T)u$, and voltage is scaled to $\varphi_0 = \hbar/2et_{\rm GL}$. Current density $\mathbf{j}$ is in units of $j_0 = c\Phi_0/(8\pi^2\lambda^2\xi)$. Parameter $\gamma = 2\tau_e\psi_0/\hbar$ characterizes the chosen material (with τ_e being the inelastic scattering time and ψ_0 being the order parameter at zero field and current) and u is the relaxation constant (i.e., the ratio between relaxation times for the phase and the amplitude of ψ). Following Ref. 16, we use $u = 5.79$ and $\gamma = 10$. Since our sample is thin enough to disallow "branching" of domains [i.e., $d \ll 800(\xi\text{-}\lambda)$],[18] both ψ and $\mathbf{j}$ can be averaged over the sample thickness.[4] The magnetic screening is calculated via the inductance $B_z = \text{rot}(\mathbf{A})|_z$ (see Ref. 4 and references therein):

$$B_z(\mathbf{r}, z = 0) = \frac{1}{c}\int Q(\mathbf{r},\mathbf{r}')g(\mathbf{r}')d^2\mathbf{r}', \qquad (3)$$

where the scalar function $g(\mathbf{r})$ is defined through $\mathbf{j}(\mathbf{r}) = \nabla \times \hat{\mathbf{z}}g(\mathbf{r})$, and the kernel Q is chosen as $Q(\mathbf{r}) = 4\pi\delta(\mathbf{r}) - d/[|\mathbf{R}|^2 + d^2/4]^{3/2}$.[4] The boundary conditions (BC) are $(\nabla - i\mathbf{A})\psi|_\perp = 0$ and $g = 0$. The transport current is introduced in the system through the BC for the vector potential, $\text{rot}\mathbf{A}|_z(y = 0, L) = \pm H_I$, where $H_I = 2\pi I/c$ is the magnetic field induced by the injected current I (with corresponding density j). We solved Eqs. (1)–(3) numerically, always starting from the fully superconducting state (i.e., $|\psi| = 1$). We then increased the current linearly over the time interval $\Delta t = 200t_{\rm GL}$, from zero to its desired value, and then conducted simulations until the dynamically stable state was reached. For facilitated control of the nucleation and further follow-up of the flux domains, we included two symmetrically located artificial defects in the sample (where $\psi = 0$; see Fig. 1).

As a representative example, we study the pattern formation in a sample with dimensions $L = 102.4\xi$, $w = 51.2\xi$, and $d = 12\xi$, and calculate the voltage during the process $[V(t)]$. The thick curve in Fig. 2 shows the $V(t)$ characteristics of the sample for the applied current density $j = 0.27$ (in the same units, the depairing current equals 0.385), for the GL parameter $\kappa = 0.4$ (roughly corresponding to Pb). This applied current induces a surface magnetic field exceeding the thermodynamic one (H_c) at the defects, so that normal domains start to nucleate (having opposite polarity on opposite sides of the sample). One expects a flux-tube "train" to form,

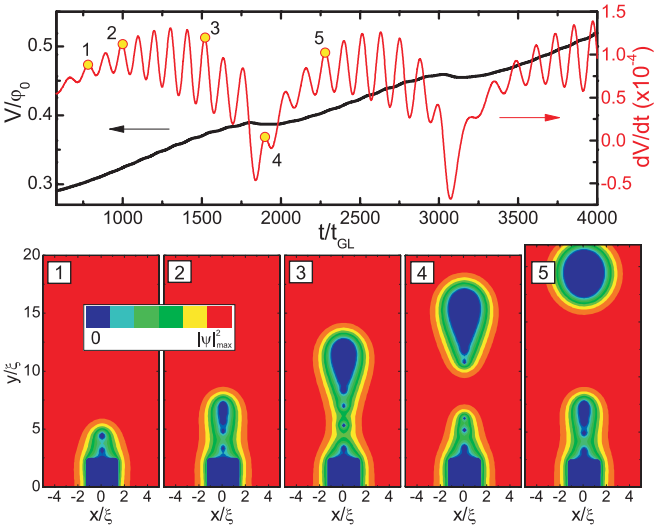

FIG. 2. (Color online) Voltage-time $[V(t)$, thicker black curve] and differential voltage-time $[dV/dt$, thinner red curve] characteristics of the sample ($\kappa = 0.4$, $L = 102.4\xi$, $w = 51.2\xi$, $d = 12\xi$, and defect size $2.4 \times 2.4\xi^2$) for the applied current density $j = 0.27j_0$, illuminating the dynamics of the discretized flux entry in the system. Panels 1–5 show snapshots of the Cooper-pair density in the vicinity of one defect (in logarithmic scale) at time intervals indicated in the main panel.

as reported in Ref. 19 for the bulk case, but neither the size of each domain, nor how each is formed, is addressed previously in the literature. Quite surprisingly, we find that flux penetrates the sample *as singly quantized vortices* (visible in panels 1–4 in Fig. 2; see also Supplemental Material)[20]—a property typical for type-II superconductors. The notion of a normal domain is only restored at a distance of $\sim 15\xi$ from the sample boundary (panel 5), which is consistent with the predictions of Ref. 13. Although single vortices do merge into a droplet due to their positive interface energy (panels 2 and 3), each individual vortex entry leaves a trace in the $V(t)$ curve, which is more pronounced in the differential voltage dV/dt (thin red curve in Fig. 2). The final "break-off" of the flux domain from the surface defect (the first domain containing 11 flux quanta, the subsequent ones containing 10) gives a more noticeable cusp in the $V(t)$ curve, and the domain is further driven by the Lorentz force (panel 5) towards the flux domains of opposite polarity coming from across the sample. While annihilation is clearly the most likely scenario, one faces another fundamental question of how the flux and the "anti"flux domain can annihilate while preserving their flux quantization during the process. Once more, the answer lies in discretization, as annihilation occurs one by one as a *vortex-antivortex pair* at a time. We show this in Fig. 3(a), which is actually a temporal extension of Fig. 2. Note that the measured voltage across the sample generally increases during the nucleation and motion of domains, but once domains meet their counterparts of opposite polarity, the singly quantized annihilation starts, which leaves an oscillatory trace on a now generally decreasing voltage [see Fig. 3(a), panels 1–4, and Supplemental Material)[21]—where each peak in the $V(t)$ curve corresponds to the annihilation of a single vortex-antivortex pair. When annihilation is complete, the voltage increases

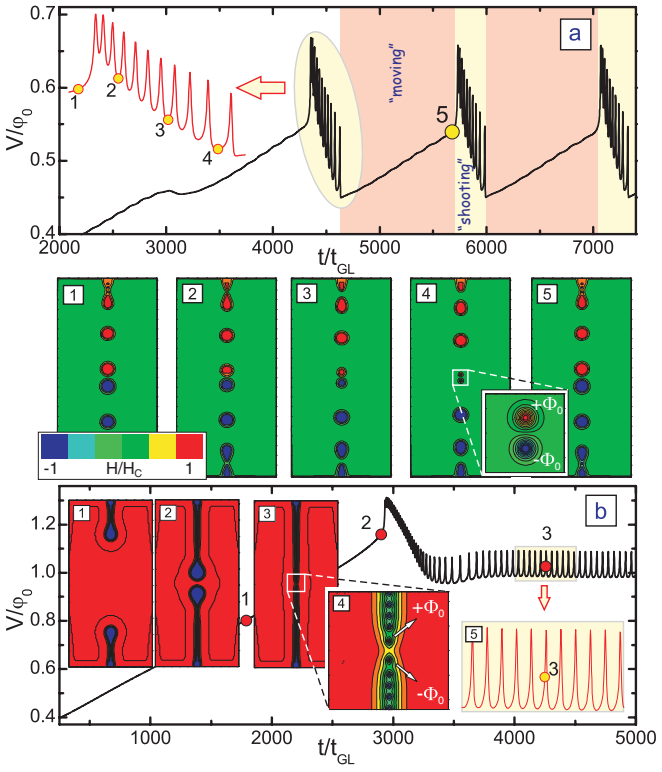

FIG. 3. (Color online) Continued $V(t)$ curves of the sample in Fig. 2 for (a) $j = 0.27 j_0$ and (b) $j = 0.34 j_0$. Panels 1–5 show snapshots of the local magnetic field, $B_z(\mathbf{r})$ (linear scale), at time intervals indicated in (a). Insets 1–4 in (b) show informative snapshots of $|\psi|^2$ (in logarithmic scale). Inset 5 in (b) and the only inset in (a) show zooms of the $V(t)$ curves, for a clearer link of the B_z and $|\psi|^2$ snapshots to the voltage features.

again with time until the next domains in line approach each other (panel 5) and the entire process repeats.

In summary, we identified two distinct modes in the dynamics of the flux domains: (i) a "*moving*" mode, characterized by a roughly linear increase of the voltage with very weak oscillations due to the quantized nucleation of domains and their motion, and (ii) a "*shooting*" mode, where singly quantized vortex-antivortex pairs are released from the domains to annihilate, each resulting in a very pronounced voltage peak and generally decreasing voltage. The number of sequential voltage peaks thus exactly matches the size of the flux domain, which for the parameters of the sample considered here varied between 7 and 13 with increasing current. At even larger current, the tube formation is no longer energetically favorable [see the insets 1–3 in Fig. 3(b)] and elongated stripes become a preferable domain shape. The output voltage increases linearly with time until stripes of opposite polarity reach each other (inset 2), which is when the $V(t)$ curve starts to exhibit periodic oscillations [see inset 5 in Fig. 3(b)], again due to the annihilation of singly quantized vortex-antivortex pairs [shown in inset 4 in Fig. 3(b); see also Supplemental Material[22] for animated data]. With further increasing current, the width of the normal channels increases but annihilation nevertheless still occurs through discrete single vortex-antivortex pairs, though with higher frequency. We conclude that Φ_0-*discretized dynamics is fundamental and general*, being independent of the magnitude of the current and the shape and size of the IS domains. Thus, our simulations confirm that singly quantized vortices are the building blocks for the IS flux structures, which is rather similar to the model proposed by Goren and Tinkham.[23]

In a real sample, the opposite flux domains induced by the current will rarely have an identical size and the same nucleation dynamics due to the always present edge imperfections. To address this to some extent, we conducted simulations for the same sample as in Fig. 2, but with defect sizes for nucleation of flux domains on the sample edges that were different ($1.8\xi \times 1.8\xi$ and $2.4\xi \times 2.4\xi$, respectively). Motivated by the real-time Hall probe measurements of Ref. 3, for the given injected current, we calculate the magnetic flux through a Hall bar ($10 \times 10\xi^2$ large), placed at $1/4$ of the flux trajectory across the sample [$(x,y) = (0, L/4)$, indicated by white squares in panels 1–6 of Fig. 4].[28] Such locally measured magnetization is plotted vs time in Fig. 4, for different values of the injected current.

For weaker driving currents [Fig. 4(a)], flux tubes enter only from one side of the sample (at the larger defect of the two). Upon flux entry, the field at the sample edge decreases, and then restores again after entered tubes have

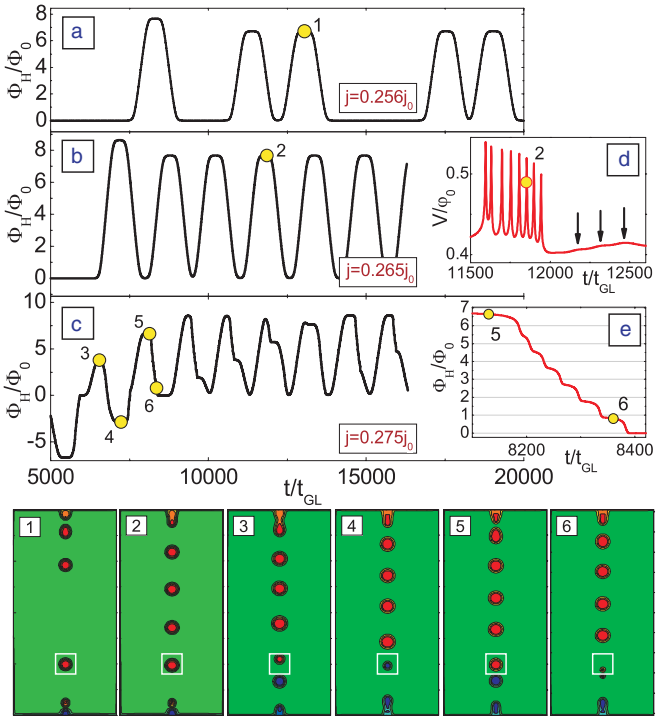

FIG. 4. (Color online) (a)–(c) Magnetization vs time response [calculated as the magnetic flux Φ_H through a Hall probe of size $10 \times 10\xi^2$ located at $(0, L/4)$] of the sample in Fig. 2 but with defects of size $2.4\xi \times 2.4\xi$ (top end) and $1.8\xi \times 1.8\xi$ (bottom end), for different values of the applied current. Inset (d) shows the voltage across the sample during the Φ_0-discretized expulsion of one of the flux tubes (large oscillations) overlapping with Φ_0-discretized flux entry on the opposite side (small oscillations highlighted by arrows). Inset (e) shows the magnetic response of the singly quantized annihilation of the flux domains. Panels 1–6 are contour plots of the magnetic field, depicting the behavior of the domains at times indicated in (a)–(e).

moved away under the driving force (see panel 1 in Fig. 4). This causes a multiperiodic flux entry, and a multiperiodic Hall response—directly corresponding to the measurements presented in Fig. 2(a) in Ref. 3. At larger currents, a shorter time is needed between subsequent flux entries, and the flow of tubes becomes periodic (panel 2) with an equitemporal magnetic response shown in Fig. 4(b). Note that in this case, we still have only flux tubes of positive polarity, entering on one side, and leaving on the other side, of the sample. Both entry and exit are Φ_0 discretized with corresponding voltage oscillations having weak amplitudes for each Φ_0 entry, and larger amplitudes for each Φ_0 exit. These oscillations often overlap, as shown in Fig. 4(d). Supplemental Material[24,25] directly show the dynamics of the flux trains for the above-discussed regimes.

With a further increase of the applied current, the flux domains start to nucleate also at the smaller defect (having opposite polarity; see panel 3 in Fig. 4), which makes the Hall response *entirely aperiodic* [shown in Fig. 4(c)]. The reason for this is the dynamic change of the annihilation point of the domains with respect to the Hall probe (see Supplemental Material)[26] as a consequence of the different size and different mobility of the annihilating flux domains. Note that qualitatively similar behavior of Hall voltage vs time was obtained in the experiment of Ref. 3, which we explain as due to the nontrivial annihilation dynamics of the flux domains. Note, however, that regardless of the annihilation point and its motion, the annihilation process remains *discretized* in individual vortex-antivortex pairs, which we find to be detectable also in magnetometry [see the steplike magnetic response depicted in Fig. 4(e)] in cases when the annihilation point is in close proximity to the Hall probe.

In summary, we showed that flux penetration, annihilation, and exit in a current-carrying *type-I* superconducting slab all occur in the form of *singly quantized* vortices, regardless of the shape and size of the flux domains in the intermediate state. In other words, even when the subdivision of the domains to individual flux quanta is not obvious, it becomes visible in dynamic processes. Revealed discrete dynamics, each flux quantum at a time, results in a measurable electronic and magnetic response of the sample. This will undoubtedly prove useful in further experiments, where more peculiarities of the type-I intermediate state can be expected—having patterns often similar to those observed in various biological and physicochemical systems,[27] but with the underlying quantized nature bound to produce exciting differences.

This work was supported by the Belgian Science Policy (IAP), the Flemish Science Foundation (FWO-Vl), and the collaborative project FWO-MINCyT (Project No. FW/08/01). G.R.B. and A.D.H acknowledge support from FWO-Vl. A.D.H. and D.D. acknowledge support from CONICET, CNEA, and ANPCyT (Grant No. PICT07-824).

*francois.peeters@ua.ac.be

[1] R. Prozorov, A. F. Fidler, J. R. Hoberg, and P. C. Canfield, Nature Phys. **4**, 327 (2008).
[2] R. Prozorov, Phys. Rev. Lett. **98**, 257001 (2007); R. Prozorov, R. W. Giannetta, A. A. Polyanskii, and G. K. Perkins, Phys. Rev. B **72**, 212508 (2005).
[3] S. B. Field and G. Stan, Phys. Rev. Lett. **100**, 077001 (2008).
[4] A. D. Hernandez and D. Domínguez, Phys. Rev. B **72**, 020505(R) (2005).
[5] G. R. Berdiyorov, A. D. Hernandez, and F. M. Peeters, Phys. Rev. Lett. **103**, 267002 (2009).
[6] M. A. Engbarth, S. J. Bending, and M. V. Milošević, Phys. Rev. B **83**, 224504 (2011).
[7] R. P. Huebener, *Magnetic Flux Structures in Superconductors* (Springer-Verlag, New York, 1979).
[8] L. D. Landau, Sov. Phys. JETP **7**, 371 (1937).
[9] R. E. Goldstein, D. P. Jackson, and A. T. Dorsey, Phys. Rev. Lett. **76**, 3818 (1996); C. R. Reisin and S. G. Lipson, Phys. Rev. B **61**, 4251 (2000); A. Cēbers, C. Gourdon, V. Jeudy, and T. Okada, *ibid.* **72**, 014513 (2005).
[10] H. Frahm, S. Ullah, and A. T. Dorsey, Phys. Rev. Lett. **66**, 3067 (1991).
[11] F. Liu, M. Mondello, and N. Goldenfeld, Phys. Rev. Lett. **66**, 3071 (1991).
[12] M. Ghinovker, I. Shapiro, and B. Ya. Shapir, Phys. Lett. A **260**, 112 (1999).
[13] H. Bokil and O. Narayan, Phys. Rev. B **56**, 11195 (1997).
[14] J. R. Hoberg and R. Prozorov, Phys. Rev. B **78**, 104511 (2008).
[15] L. Kramer and R. J. Watts-Tobin, Phys. Rev. Lett. **40**, 1041 (1978).
[16] R. J. Watts-Tobin, Y. Krähenbühl, and L. Kramer, J. Low Temp. Phys. **42**, 459 (1981).
[17] G. Blatter, M. V. Feigel'man, V. B. Geshkenbein, A. I. Larkin, and V. M. Vinokur, Rev. Mod. Phys. **66**, 1125 (1994).
[18] A. Hubert, Phys. Status Solidi **24**, 669 (1976).
[19] D. E. Chimenti and R. P. Huebener, Solid State Commun. **21**, 467 (1977).
[20] See Supplemental Material at http://link.aps.org/supplemental/10.1103/PhysRevB.85.092502 for an online video of the time evolution of the superconducting order parameter, which shows the Φ_0-discretized penetration of the flux (Fig. 2).
[21] See Supplemental Material at http://link.aps.org/supplemental/10.1103/PhysRevB.85.092502 for an online video of flux annihilation, one vortex-antivortex pair at a time [Fig. 3(a)].
[22] See Supplemental Material at http://link.aps.org/supplemental/10.1103/PhysRevB.85.092502 for an online video of discretized flux penetration and annihilation [Fig. 3(b)].
[23] R. N. Goren and M. Tinkham, J. Low Temp. Phys. **5**, 465 (1971).
[24] See Supplemental Material at http://link.aps.org/supplemental/10.1103/PhysRevB.85.092502 for an online video of multiperiodic flux entry and exit, corresponding to Fig. 4(a).
[25] See Supplemental Material at http://link.aps.org/supplemental/10.1103/PhysRevB.85.092502 for an online video of periodic flux entry and exit, corresponding to Fig. 4(b).
[26] See Supplemental Material at http://link.aps.org/supplemental/10.1103/PhysRevB.85.092502 for an online video of aperiodic flux annihilation, corresponding to Fig. 4(c).
[27] M. Seul and D. Andelman, Science **267**, 476 (1995).
[28] Our conclusions are actually independent of the chosen location of the Hall probe.